

Short Communication

Genome editing of *Nf1*, *Pten*, and *Trp53* in neonatal mice induces glioblastomas positive for oligodendrocyte lineage transcription factor 2

Hiromi Yamamoto¹, Keisuke Yamamura¹, Haruka Nagasaki¹, Takamasa Suzuki¹, Fumiko Ninomiya¹, Kenji Matsubara¹, Naomoto Harada^{1*}, and Shuichi Ohkubo¹

¹Discovery and Preclinical Research Division, Taiho Pharmaceutical Co., Ltd., 3 Okubo, Tsukuba, Ibaraki 300-2611, Japan

Abstract: To generate a mouse glioblastoma model by genome editing, we introduced Cas9 protein and guide RNAs specific for *Nf1*, *Pten*, and *Trp53* into the neonatal mouse forebrain by electroporation. We found a high incidence (approximately 90%) of glial tumor development, including glioblastomas, 15 weeks later. The histological features of the tumors were similar to those of diffuse gliomas and, in some cases, similar to human glioblastomas, with microvascular proliferation (glomeruloid structure). In addition, unlike glial fibrillary acidic protein (GFAP)-positive glioblastomas generated using a similar method in a previous model, the majority of tumor cells were positive for oligodendrocyte lineage transcription factor 2, but negative for GFAP and neurofilaments. One base pair insertions identical to those seen in a previous model were found around the target sequences in *Nf1*, *Pten*, and *Trp53*, and additional deletions were found only in *Pten*. Considering that the histological characteristics were different from those seen in the previous model, our new model provides an additional research tool to investigate the early stages of glioblastoma development. (DOI: 10.1293/tox.2021-0029; J Toxicol Pathol 2021; 34: 359–365)

Key words: glioblastoma, animal model, genome editing, *in vivo* electroporation, mouse, oligodendrocyte lineage transcription factor 2

Human glioblastoma is the most malignant primary brain tumor, and its highly infiltrative nature makes it difficult to completely resect by surgery^{1, 2}. The 2016 World Health Organization (WHO) classification divided human glioblastomas into three types: (i) glioblastoma, IDH wild-type (~90% of cases), which corresponds most frequently with the clinically defined primary or *de novo* glioblastoma in the previous WHO classification (WHO 2007)³; (ii) glioblastoma, IDH mutant (~10% of cases), which corresponds closely to the so called secondary glioblastoma; and (iii) glioblastoma, not otherwise specified⁴. *NF1*, *PTEN*, and *TP53* are the most commonly mutated tumor suppressor genes in human primary glioblastoma^{5, 6}. Various mouse glioblastoma models, such as genetically engineered models, intracranial xenograft and allograft models, patient-derived xenograft models, and chemically induced models have been reported, with each model having advantages and

disadvantages^{7, 8}. Zuckermann *et al.* established a CRISPR/Cas9-mediated glioblastoma model in mice by simultaneously disrupting *Nf1*, *Pten*, and *Trp53* by injection and electroporation (EP) of plasmid vectors into the forebrain of embryos *in utero*. However, the group did not fully elucidate the histopathological characterization of the resulting tumors⁹. In the present study, we successfully reproduced this mouse glioblastoma model not by using a plasmid vector but by directly injecting a ribonucleoprotein (RNP) complex consisting of the Cas9 protein and gRNAs specific for *Nf1*, *Pten*, and *Trp53*. Furthermore, we performed detailed histopathological and immunohistochemical (IHC) analyses of the tumors. For *in vivo* genome editing, we synthesized the following Alt-R™ CRISPR-Cas9 crRNAs (Integrated DNA Technologies, Inc., Coralville, IA, USA) to target the following sequences (Fig. 1A):

Nf1: 5'-AGTCAGCACCGAGCACAACAAGG-3'

Pten: 5'-AAAGACTTGAAGGTGTATACAGG-3'

Trp53: 5'-ACAGCCATCACCTCACTGCATGG-3'

To prepare the RNP complex, each crRNA was annealed with tracrRNA (Integrated DNA Technologies, Inc.) and then mixed with Alt-R™ S.p. Cas9 Nuclease V3 (Integrated DNA Technologies, Inc.) in phosphate-buffered saline. The final concentration was 2.5 μg/μL for each annealed gRNA and 1.8 μg/μL for Cas9 nuclease. ICR mice were purchased from Charles River Laboratories Japan (Yokohama, Japan), and the RNP complex was introduced into

Received: 11 May 2021, Accepted: 5 July 2021

Published online in J-STAGE: 23 July 2021

*Corresponding author: N Harada

(e-mail: nm-harada@taiho.co.jp)

©2021 The Japanese Society of Toxicologic Pathology

This is an open-access article distributed under the terms of the Creative Commons Attribution Non-Commercial No Derivatives

(by-nc-nd) License. (CC-BY-NC-ND 4.0: <https://creativecommons.org/licenses/by-nc-nd/4.0/>).



the right side of the forebrains of neonatal (P0) mice by EP, as previously reported¹⁰ (Fig. 1B). Before EP, the injection position was confirmed using trypan blue dye instead of the RNP complex (Fig. 1C). The EP parameters are presented in Table 1. All mice were maintained under standard housing conditions with a 12-h light/dark cycle (light phase, 8:00 am to 8:00 pm; dark phase, 8:00 pm to 8:00 am) and were fed ad libitum with a regular chow diet (CE-2; CLEA, Tokyo, Japan) until necropsy. All animal procedures were approved by the Taiho Institutional Animal Care and Use Committee. For histopathological and IHC analyses, the whole head without the mandible was fixed in 10% neutral-buffered formalin (FUJIFILM Wako Pure Chemical Corporation, Osaka, Japan), decalcified in 10% formic acid (FUJIFILM Wako Pure Chemical Corporation), trimmed cross-sectionally, and then fixed again in 10% neutral-buffered formalin. The fixed heads were embedded in paraffin, cut into 2- μ m thick sections, and stained with hematoxylin-eosin. For IHC analyses, heat-induced antigen retrieval was performed in citrate buffer at pH 6 (LSI Medience Corporation, Tokyo, Japan). The following primary antibodies were used: anti-oligodendrocyte lineage transcription factor 2 (anti-Olig2; EPR2673, 1:250; Abcam, Cambridge, UK), anti-GFAP (EPR1034Y, 1:200, Abcam), anti-ionized calcium binding adapter protein (anti-Iba-1; 019-19741, 1:500, FUJIFILM Wako Pure Chemical Corporation)¹¹, anti-neurofilament (anti-NF; ab8135, 1:1,000, Abcam), and anti-Ki67 (SP6, 1:100, Abcam). The sections were visualized using the polymeric method (Nichirei-Histofine Simple Stain MAX PO[®]; Nichirei Biosciences, Tokyo, Japan). The extracranial mass was incubated at 55 °C overnight in lysis buffer (50 mM Tris-HCl [pH 8.0], 10 mM EDTA, 100 mM NaCl, 1% SDS, 1% proteinase K), and genomic DNA was then purified by phenol/chloroform extraction. Fragments of *Nf1*, *Pten*, and *Trp53* were amplified by PCR using 35 cycles of 94 °C for 30 s, 60 °C for 30 s, and 72 °C for 1 min. The following primers were used:

Nf1-Fw: 5'-TCTTACTTTGTAGCTAGAGGGACATAG-3'
Nf1-Rv: 5'-AATTAATAAGAGAAGCTTCAACGGG-3'
Pten-Fw: 5'-ACTGTGGCAGTAGGAACCTTATAGA-3'
Pten-Rv: 5'-CCTTGTACTGTAATACAAGCCAGAG-3'
Trp53-Fw: 5'-AGAAGTTTGAGGTCATCATTGACTAC-3'
Trp53-Rv: 5'-GTTCAGGGCAAACTAACTCTGA-3'

The PCR products were sequenced after cloning to a plasmid vector using a TOPO-TA cloning kit (Thermo Fisher Scientific K.K., Tokyo, Japan).

Eight out of nine mice were sacrificed at 15 weeks after EP (15 weeks of age) to monitor tumor development, and one mouse was necropsied on day 39 after EP (5 weeks of

age) because of a firm protruding mass on the right side of the forehead. Upon histopathological evaluation, seven of the eight mice sacrificed at 15 weeks after EP had developed diffusely infiltrating tumors, and the remaining mouse had developed hyperplasia. The tumors were mainly located in the right brain where the RNP complex had been injected (Fig. 2A); however, in some cases, the tumors had spread through the corpus callosum, striatum, or ventricle to the opposite side (Fig. 2H). Proliferating tumor cells had polymorphic features, including variably shaped nuclei (mainly round to elongated, but sometimes irregularly shaped and multinucleated) and indistinct cytoplasmic borders (Fig. 2B, I). Most tumors had malignant histological features, such as hemorrhage, neuronal satellitosis, and Homer Wright rosettes, and most showed invasion into the perivascular and ventricular spaces, meninges, and bone marrow (Fig. 3B–F). However, only three tumors had microvascular proliferations (glomeruloid structures; Fig. 3A). For further characterization of the tumors, tissue sections were stained for GFAP, as a marker of astrocytes; Olig2, as a marker of oligodendrocytes and glial progenitors¹²; NF, as a marker of neurons; Iba-1, as a marker of microglia¹³; and Ki67, as a marker of proliferating cells. In the seven tumors in the brain parenchyma, the main population of neoplastic cells was positive for Olig2 (Fig. 2C, J) and Ki67 (Fig. 2D, K) but negative for NF (Fig. 2E, L). Although GFAP-positive stellate cells with prominent processes were distributed within or along the edge of the tumors (Fig. 2F, M), the morphological features and distribution of these cells indicated that they were reactive astrocytes¹⁴. Similarly, Iba-1-positive cells with increased cellularity, either in or scattered around the tumor area (Fig. 2G, N), appeared to be reactive microglia^{15, 16}. Based on these histological and IHC results, we diagnosed the tumors as gliomas (n=4), including glioblastomas (n=3; Tables 2 and 3).

In the mouse necropsied at 5 weeks of age, approximately half of the mass on the forehead was excised for genetic analyses, and the rest of the head was subjected to histological evaluation. The latter confirmed an extracranial tumor that was separated from the brain parenchyma (Fig. 4A) and included two types of cells: (i) interlacing bundles of spindle cells with atypical round to oval nuclei, some of which were undergoing mitosis (Fig. 4B), and (ii) stellate cells with abundant eosinophilic cytoplasm harboring round to oval-shaped, and sometimes multiple, nuclei (Fig. 4C). The spindle cells consisted of admixed Olig2-positive cells and Iba-1-positive cells, and atypical nuclei were positive for Olig2 (Fig. 4D, E). Stellate cells were positive for GFAP (Fig. 4F). Combined with the morphological find-

Table 1. Electroporation Parameters

Poring pulse					Transfer pulse					Resistance (Ω)
Voltage (V)	Width (ms)	Interval (ms)	Decay Rate (%)	No. of pulses	Voltage (V)	Width (ms)	Interval (ms)	Decay Rate (%)	No. of pulses	
40 or 60	30	50	10	+3	8	30	50	40	\pm 3	0.7–1.1

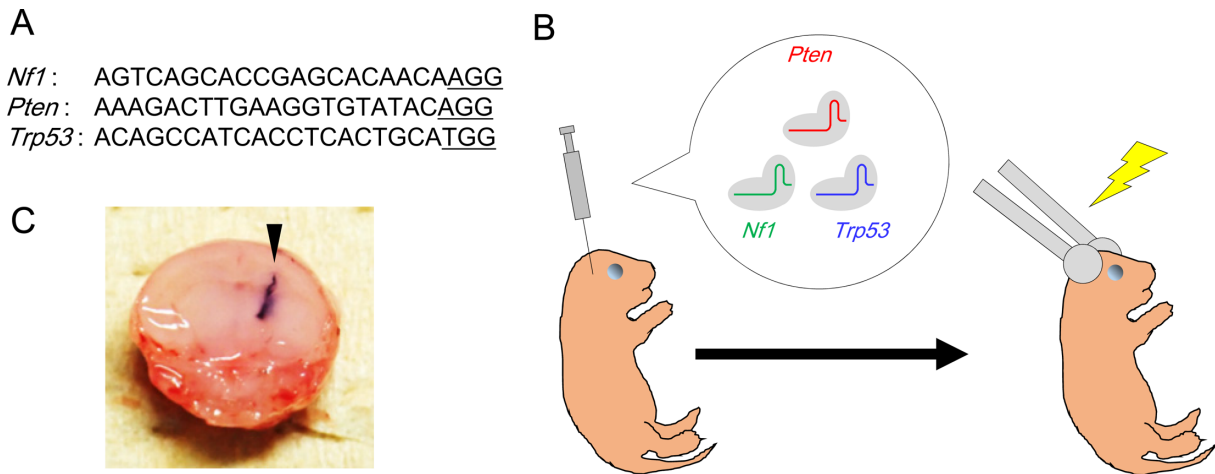


Fig. 1. *In vivo* genome editing. (A) Sequences targeting *Nf1*, *Pten*, and *Trp53*. The underlined bases represent the PAM sequence. (B) A mixture of ribonucleoprotein complexes was injected into the forebrains of neonatal mice (P0), and electroporation was performed. (C) The injection position was confirmed by injecting trypan blue dye (arrowhead).

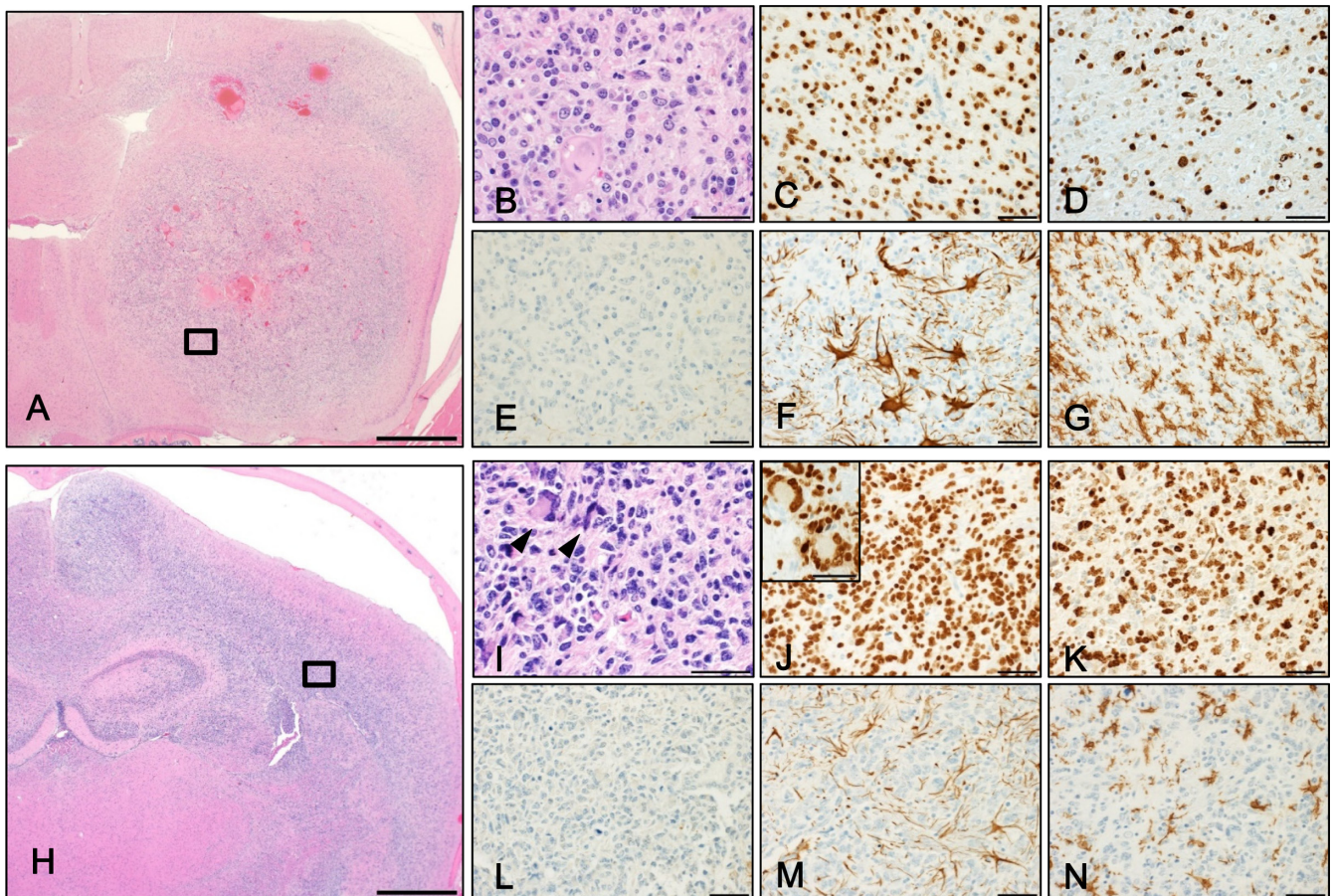


Fig. 2. Immunohistochemical analysis of glioblastomas in two mice. (A, H) Low magnification of hematoxylin-eosin (HE) staining of the glioblastoma. Diffuse infiltrative growth was seen. (B, I) Higher magnification of HE staining of the glioblastoma. Variably shaped nuclei (round to elongated, sometimes irregularly shaped) and indistinct cell borders were seen in neoplastic cells. The arrowhead indicates a multinucleated giant cell. (C, J) Oligodendrocyte lineage transcription factor 2 (Oligo2) staining. (D, K) Ki67 staining. (E, L) Neurofilament (NF) staining. Neoplastic cells were positive for Oligo2 (including multinucleated giant cell shown in the inset of J) and Ki67, but negative for NF. (F, M) Glial fibrillary acidic protein (GFAP) staining. GFAP-positive hypertrophic stellate cells were considered to be reactive astrocytes. (G, N) Ionized calcium binding adapter protein (Iba-1) staining. Ramified, bushy, hypertrophic, and amoeboid Iba-1-positive cells were considered to be reactive microglia. (A, H) bar = 1 mm; (B to G) and (I to N), bar = 50 μ m. Figure parts B to G and I to N correspond to the areas indicated by the squares in (A) and (H), respectively.

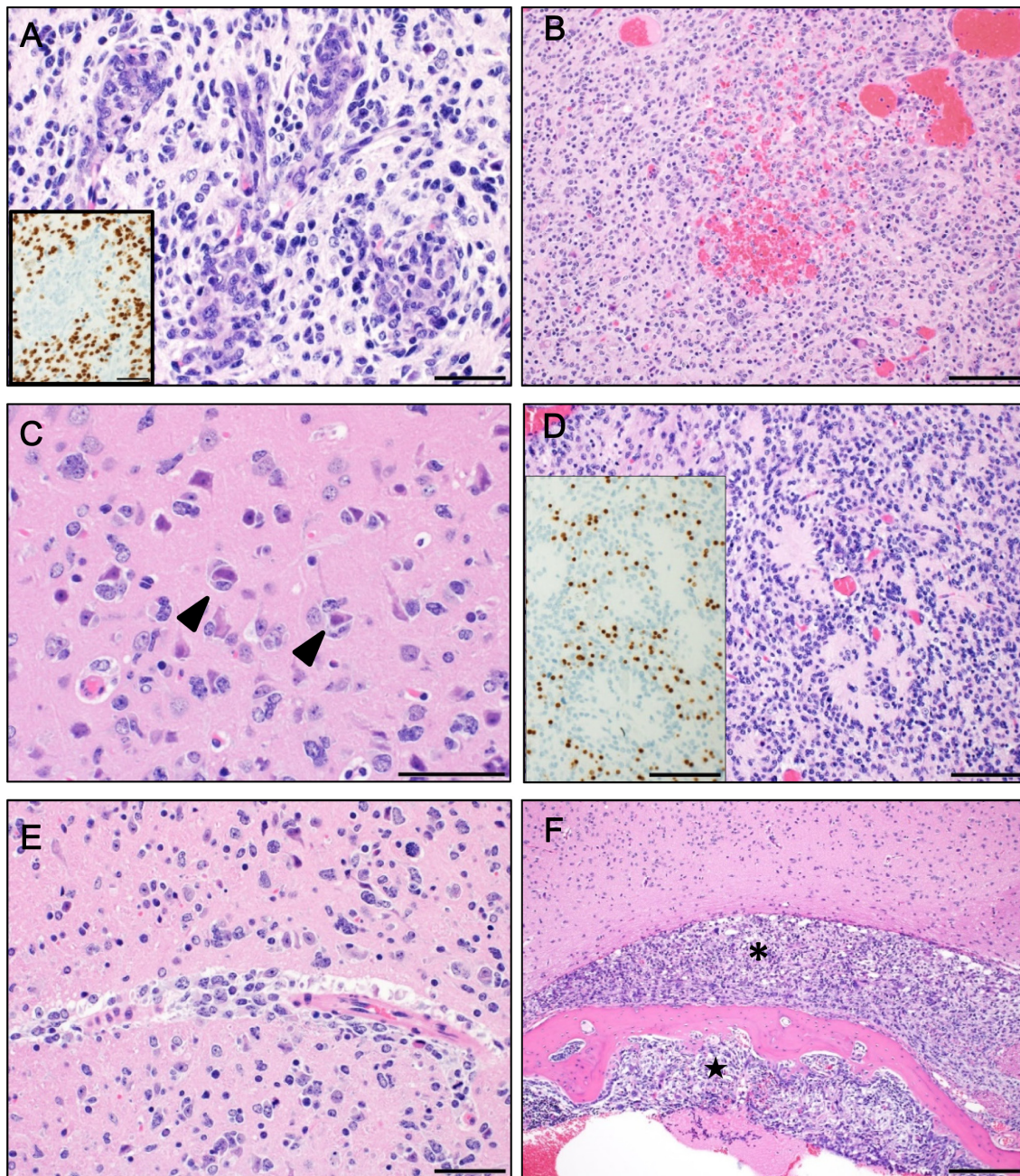


Fig. 3. Histology of the glioblastomas in three mice. (A) Glomeruloid microvascular proliferation (hematoxylin-eosin [HE] staining). The inset shows that neoplastic cells were positive for oligodendrocyte lineage transcription factor 2 (Olig2), but endothelial cells were not. (B) Hemorrhage and dilated microvessels (HE staining). (C) Satellitosis at the periphery (arrowheads; HE staining). (D) Homer Wright rosettes (HE staining). The inset shows that rosettes were negative for Olig2. (E) Invasion into perivascular spaces (HE staining). (F) Invasion into meninges (asterisk) and bone marrow (star; HE staining). (A, C, E), bar = 50 μ m; (B, D), bar = 100 μ m; (F), bar = 200 μ m.

Table 2. Incidence of Tumors and Hyperplasia

Age (w)	Location	Diagnosis	No. of mice
5	Extracranial	Glioma	1
15	Brain parenchyma	Glioblastoma	3
		Glioma	4
		Hyperplasia	1
Total			9

ings (Fig. 4C), some GFAP-positive cells appeared to have multiple nuclei. Some other GFAP-positive cells showed an astrocyte-like appearance (data not shown). Both spindle and stellate cells were negative for NF (Fig. 4G). These results suggested that this tumor may be an Olig2-positive, GFAP-positive glioma derived from the brain parenchyma, although the admixed Iba-1 positive cells seemed to be macrophages. No morphological changes were detected in the cerebrum of this animal (data not shown). The decalcifica-

tion step with 10% formic acid was not required for the extracranial tumor, which enabled us to purify genomic DNA from the tumor and determine whether indel mutations were present. One base pair insertions were found around the CRISPR/Cas9 target sequences in *Nf1*, *Pten*, and *Trp53* and these insertions were identical to those previously reported in another model⁹. Additional deletions ($\Delta 4$, $\Delta 14$, and $\Delta 10$ bp) were also found, but only in *Pten* (Fig. 4H). These data suggested that the frameshift mutations caused by genome editing resulted in a loss of protein expression, which led to gliomagenesis.

In this study, we simultaneously edited three tumor suppressor genes (*Nf1*, *Pten*, and *Trp53*) in the forebrains of neonatal (P0) mice and succeeded in producing glial tumors that were positive for Olig2 and negative for GFAP, Iba-1, and NF. Some tumors (5/9) were diagnosed as gliomas based on histological features (nuclear atypia, mitotic activity, satellitosis, invasion into the perivascular space, appearance of multinucleated giant cells, and microglial infiltration). These Olig2-positive tumors may have been oligodendrogliomas, although this diagnosis seems unlikely because they did not show the typical “honeycomb” pattern of oligodendrogliomas. In addition to the above-mentioned histological features, some tumors (3/9) were diagnosed as glioblastomas based on glomeruloid microvascular proliferation, which is a histological hallmark that distinguishes glioblastomas from lower-grade gliomas in humans^{2, 17}. Notably, microglial infiltration was prominent, as reported in human glioblastomas (up to 30% of the entire tumor mass)¹⁸. In one of the glioblastomas, Homer Wright rosettes were found focally in the Olig2-positive tumor area, but the rosettes were negative for Olig2 and GFAP. These findings are similar to the pattern so called “human glioblastoma with primitive neuronal component”, which typically display the loss of glial marker expression⁴. These results strongly indicated that our model mimicked the histopathological features of human gliomas and glioblastomas.

The extracranial tumor that developed in one mouse consisted of Olig2-positive neoplastic cells, GFAP-positive cells, and Iba1-positive cells. Unlike intracranial tumors, it seems unlikely that normal astrocytes and normal microglia were present in the extracranial tumors. Therefore, we concluded that some of the GFAP-positive cells were neoplastic cells, and the Iba-1 positive cells were macrophages. Because mutations in the targeted genes were found in the extracranial tumor, it was likely that genome editing occurred in the brain parenchymal cells. These cells may have exuded out of the skull and proliferated in the extracranial region, which was then infiltrated by macrophages. Based on these histological and molecular features, we diagnosed the extracranial tumor as a glioma, although we did not observe any contact between the tumor and the brain parenchyma.

Zuckerman *et al.* reported that simultaneous mutations in *Nf1*, *Pten*, and *Trp53* genes in the mouse forebrain results in highly aggressive tumors resembling human glioblastomas 6 to 14 weeks after *in utero* EP. The histological features of their glioblastoma model, such as highly prolifera-

tive pleomorphic neoplastic cells, multinucleated cells, and microvascular proliferation, were almost the same as those found in our model; however, they also observed focal necrosis, which was barely found in our model. In addition, the incidence of glioblastoma was higher in their model (8/8) than in our model (3/9). Furthermore, in their model, the neoplastic cells were GFAP-positive, but in our model they were Olig2-positive (except for the extracranial tumors). These discrepancies may be partly explained by differences in the timing of genome editing; that is, at the neurogenesis stage (E14.5) in their model and the gliogenesis stage (P0) in our model. Neural stem cells distributed in the ventricular and subventricular zones of the lateral ventricles continuously differentiate into neuronal cells from E10 to E17.5, and then to glial cells from E17.5 to P10¹⁹. Thus, the developmental stage of genome-edited cells may affect the genesis of glioblastoma. In addition, neither model analyzed time-dependent changes in glioblastoma incidence. Furthermore, pseudopalisading necrosis can be caused by hypoxia due to compromised vascular function and obstruction of tumor blood vessels², so the glioblastoma in our model may have led to a hypoxic condition if we had observed the mice for a longer period. Therefore, we sought to determine whether the glioblastoma incidence increased and pseudopalisading necrosis was observed after a longer period than the 15 weeks used in our model.

Non-homologous end joining-mediated repair should randomly induce various mutations²⁰. Our finding of identical mutations (1 bp insertions) to those seen in the previous model in the CRISPR/Cas9 target sequences of *Nf1*, *Pten*, and *Trp53* in the extracranial tumor, despite using a different CRISPR/Cas9 delivery system (RNP complexes) than the previous model (plasmid vector)⁹, was noteworthy. Although we were unable to analyze the mutations in the intracranial glial tumors because of DNA degradation caused by decalcification with formic acid, the same mutations may have also occurred in these tumors. We are currently performing a study to investigate this possibility and monitor tumor progression for longer than 15 weeks after EP.

In conclusion, we successfully developed a mouse glioma/glioblastoma model using *in vivo* EP of RNP complexes targeting *Nf1*, *Pten*, and *Trp53* into the forebrains of neonatal mice. The histological features of the tumors mimicked those commonly found in diffuse gliomas and glioblastomas in humans. Because our model used a different method and timing of genome editing than the previously reported model and resulted in unique histological characteristics, it represents an additional research tool to investigate the early stage of gliomagenesis.

Disclosure of Potential Conflicts of Interest: All authors are employees of Taiho Pharmaceutical Co., Ltd., Tsukuba, Ibaraki, Japan.

References

1. Fan X, Xiong Y, and Wang Y. A reignited debate over the cell(s) of origin for glioblastoma and its clinical implications. *Front Med.* **13**: 531–539. 2019. [[Medline](#)] [[CrossRef](#)]
2. Hambardzumyan D, and Bergers G. Glioblastoma: defining tumor niches. *Trends Cancer.* **1**: 252–265. 2015. [[Medline](#)] [[CrossRef](#)]
3. Louis DN, Ohgaki H, Wiestler OD, Cavenee WK, Burger PC, Jouvet A, Scheithauer BW, and Kleihues P. The 2007 WHO classification of tumours of the central nervous system. *Acta Neuropathol.* **114**: 97–109. 2007. [[Medline](#)] [[CrossRef](#)]
4. Louis DN, Perry A, Reifenberger G, von Deimling A, Figarella-Branger D, Cavenee WK, Ohgaki H, Wiestler OD, Kleihues P, and Ellison DW. The 2016 World Health Organization Classification of Tumors of the Central Nervous System: a summary. *Acta Neuropathol.* **131**: 803–820. 2016. [[Medline](#)] [[CrossRef](#)]
5. Koo H, Choi SW, Cho HJ, Lee IH, Kong DS, Seol HJ, Lee JI, Choi JW, Sa JK, and Nam DH. Ethnic delineation of primary glioblastoma genome. *Cancer Med.* **9**: 7352–7359. 2020. [[Medline](#)] [[CrossRef](#)]
6. McLendon R, Friedman A, Bigner D, Van Meir EG, Brat DJ and Cancer Genome Atlas Research Network. Comprehensive genomic characterization defines human glioblastoma genes and core pathways. *Nature.* **455**: 1061–1068. 2008. [[Medline](#)] [[CrossRef](#)]
7. Kijima N, and Kanemura Y. Mouse Models of Glioblastoma. In: *Glioblastoma*, S De Vleeschouwer (ed). Codon Publications, Brisbane. 131–139. 2017.
8. Miyai M, Tomita H, Soeda A, Yano H, Iwama T, and Hara A. Current trends in mouse models of glioblastoma. *J Neurooncol.* **135**: 423–432. 2017. [[Medline](#)] [[CrossRef](#)]
9. Zuckermann M, Hovestadt V, Knobbe-Thomsen CB, Zapatka M, Northcott PA, Schramm K, Belic J, Jones DT, Tschida B, Moriarity B, Largaespada D, Roussel MF, Korshunov A, Reifenberger G, Pfister SM, Lichter P, Kawauchi D, and Gronych J. Somatic CRISPR/Cas9-mediated tumour suppressor disruption enables versatile brain tumour modelling. *Nat Commun.* **6**: 7391. 2015. [[Medline](#)] [[CrossRef](#)]
10. Boutin C, Diestel S, Desoeuvre A, Tiveron M-C, and Cremer H. Efficient in vivo electroporation of the postnatal rodent forebrain. *PLoS One.* **3**: e1883. 2008. [[Medline](#)] [[CrossRef](#)]
11. Furukawa S, Nagaike M, and Ozaki K. Databases for technical aspects of immunohistochemistry. *J Toxicol Pathol.* **30**: 79–107. 2017. [[Medline](#)] [[CrossRef](#)]
12. Marshall CA, Novitsch BG, and Goldman JE. Olig2 directs astrocyte and oligodendrocyte formation in postnatal sub-ventricular zone cells. *J Neurosci.* **25**: 7289–7298. 2005. [[Medline](#)] [[CrossRef](#)]
13. Sacaan A, Thibault S, and Khan KN. Central nervous system tumors in 2-year rat carcinogenicity studies: perspectives on human risk assessment. *J Toxicol Sci.* **44**: 643–655. 2019. [[Medline](#)] [[CrossRef](#)]
14. Sofroniew MV, and Vinters HV. Astrocytes: biology and pathology. *Acta Neuropathol.* **119**: 7–35. 2010. [[Medline](#)] [[CrossRef](#)]
15. Bryukhovetskiy I, Manzhulo I, Mischenko P, Milkina E, Dyuzen I, Bryukhovetskiy A, and Khotimchenko Y. Cancer stem cells and microglia in the processes of glioblastoma multiforme invasive growth. *Oncol Lett.* **12**: 1721–1728. 2016. [[Medline](#)] [[CrossRef](#)]
16. Wyatt-Johnson SK, Herr SA, and Brewster AL. Status epilepticus triggers time-dependent alterations in microglia abundance and morphological phenotypes in the hippocampus. *Front Neurol.* **8**: 700. 2017. [[Medline](#)] [[CrossRef](#)]
17. Wesseling P, Kros JM, and Jeuken JWM. The pathological diagnosis of diffuse gliomas: towards a smart synthesis of microscopic and molecular information in a multidisciplinary context. *Diagn Histopathol.* **17**: 486–494. 2011. [[CrossRef](#)]
18. Russo CD, and Cappoli N. Glioma associated microglia/macrophages, a potential pharmacological target to promote antitumor inflammatory immune response in the treatment of glioblastoma. *Neuroimmunol Neuroinflamm.* **5**: 36. 2018. [[CrossRef](#)]
19. Bronstein R, Kyle J, Abraham AB, and Tsirka SE. Neurogenic to gliogenic fate transition perturbed by loss of HMGB2. *Front Mol Neurosci.* **10**: 153. 2017. [[Medline](#)] [[CrossRef](#)]
20. Mali P, Yang L, Esvelt KM, Aach J, Guell M, DiCarlo JE, Norville JE, and Church GM. RNA-guided human genome engineering via Cas9. *Science.* **339**: 823–826. 2013. [[Medline](#)] [[CrossRef](#)]